Condensation mechanisms of an arsenic-rich vapor on GaAs (001) surfaces

D. A. Murdick* and H. N. G. Wadley
School of Engineering and Applied Science, University of Virginia, Charlottesville, Virginia 22904, USA

X. W. Zhou
Mechanics of Materials Department, Sandia National Laboratories, Livermore, California 94550, USA
(Received 17 November 2005; revised manuscript received 12 February 2007; published 21 March 2007)

The homoepitaxial assembly of a (001) GaAs surface from atomic gallium and molecular As_2 vapor fluxes has been investigated with molecular dynamics simulations using a recently developed bond-order potential. The approach enables dynamic atomic assembly events to be observed as atoms condense to form thin film structures. During simulation of epitaxial growth, we observed a temperature-dependent arsenic solubility limit consistent with experimental results. The As_2 sticking probabilities and dynamic dimer-surface binding states for both gallium- and arsenic-terminated (001) surfaces were also explored. On gallium-terminated surfaces, significant switching between two weakly bound precursor states and an intermediate chemisorbed state was observed during the surface diffusion of arsenic dimers. The switching frequency was strongly temperature dependent. The arsenic dimers bound to arsenic-terminated surfaces were found to be more likely to desorb (instead of diffuse) when thermally perturbed from their adsorption sites. This sticking probability was strongly dependent on surface temperature, atomic adsorption site environment, and the orientation of the incoming dimer.

DOI: 10.1103/PhysRevB.75.125318 PACS number(s): 81.05.Ea, 81.15.Aa, 68.43.Mn, 68.43.Pq

I. INTRODUCTION

Gallium arsenide thin films are typically grown from atomic gallium and molecular arsenic (As_4 or As_2) fluxes using molecular beam epitaxy (MBE) in an ultrahigh vacuum environment.[1,2] The high-temperature (HT) epitaxial growth of GaAs on the (001) surface is usually conducted between 855 and 875 K, but the region can extend from 775 to 915 K.[3] During HT growth, experiments have shown that the arsenic dimer sticking probability is almost zero in the absence of an exposed population of surface gallium atoms,[4] while the gallium sticking probability remains near unity.[5] In the HT region, the growth rate is therefore controlled by the gallium flux and stoichiometric films are only formed under As:Ga flux ratios that are much greater than unity.[6,7] Oscillations in reflection high-energy electron diffraction (RHEED) patterns and scanning tunneling microscopy (STM) have identified the range of processing conditions that facilitate two-dimensional, layer-by-layer growth via lateral step propagation.[8] This is the growth mode associated with highly crystalline lattice structures and low atomic defect concentrations.[3]

GaAs thin films can also be deposited at low temperatures in the 500–625 K range.[9] RHEED observations indicate that as the growth temperature is decreased from HT conditions while maintaining a high As:Ga flux ratio, the step flow mode of growth ceases at 773 K.[9] The electrical and optical characteristics are adversely affected as the temperature is decreased to 725 K and below.[10] As the temperature is further reduced, highly defective thin film structures form.[9] These temperature-dependent changes in the low-temperature (LT) GaAs film properties have been correlated with excess arsenic incorporation in the as-grown films.[11] The amount of excess arsenic that can be trapped in the as-grown GaAs lattice increases as the temperature decreases.[9] At 525 K, the arsenic solubility limit is between 1 and 1.5 %.[12] The As_2 sticking ratio has also been observed to strongly increase as the temperature is decreased in this regime.[13] As a result, stoichiometric LT GaAs films can only be grown by decreasing the As:Ga flux ratio toward unity.[10,14]

The atomic scale assembly phenomena responsible for these experimental observations are not fully understood. The experimental study of these processes during growth of a thin film is difficult because of limited spatial (single atom dynamics) and temporal (short relaxation times) measurement resolution. Computational methods provide a route for developing an understanding of assembly dynamics. The atomic assembly processes that control film composition, growth mode, and thus film quality during the vapor phase growth of GaAs can be probed by a variety of computational models provided they capture the essential physics involved in vapor/surface interactions. However, all the candidate computational methods suffer from drawbacks and can address only limited aspects of the vapor deposition process.

Simulations using kinetic Monte Carlo (kMC) algorithms seek to model the thermally activated surface diffusion process that controls island nucleation and growth.[15,16] These statistical methods can be used to investigate atomic assembly processes, provided an appropriate activation barrier database exists.[15,16] This becomes increasingly problematic for off-lattice models and multicomponent systems. These techniques are able to address relevant assembly time scales, but the simplifications introduced by using a small set of precalculated atom jump paths and the removal of environmentally dependent atomic forces limit the effectiveness of the approach. Density functional theory (DFT) can be used to calculate surface binding energies, activation energy barriers, and surface diffusion jump paths.[17–19] Additionally, the equations of motion can be integrated from the Lagrangian for both electronic wave functions and atomic coordinates using *ab initio* molecular dynamics (MD).[20] The computational expense of this method restricts its use for very short (on the

order of tens of picoseconds) simulations of single event dynamics with hundreds of atoms.[21,22]

The MD technique used here is based upon interatomic potentials and enables the study of surface atomic assembly processes for times that vary from nanoseconds to microseconds (depending upon the available computational resources). The accuracy of predicted assembly mechanisms and kinetics are governed by the degree to which the potential models the angular and radially dependent forces between atoms during the making and breaking of bonds on a surface. MD methods have been used to simulate GaAs surface diffusion and thin film growth using empirical Tersoff and/or Stillinger-Weber interatomic potentials.[23,24] However, the limited validity of these potentials has significantly restricted the use of this approach to date.[25]

Here we use a recently derived analytic bond-order potential (BOP) that has been shown to model well the properties of GaAs clusters, bulk lattices, point defects, and surfaces.[26] We use this GaAs BOP to conduct MD simulations of the homoepitaxial growth of (001) GaAs surfaces and assess its validity by comparing results with experimental studies of LT GaAs growth. The atomic-scale assembly mechanisms active on both gallium- and arsenic-terminated (001) surfaces are then studied in detail to investigate the dynamic phenomena following arsenic dimer impacts over a wide range of surface temperatures. This MD study of surface kinetics opens a window into GaAs surface dynamics over length and time scales that were not previously accessible.

II. COMPUTATIONAL METHODS

MD simulations were performed using a BOP recently described and parametrized for the GaAs system.[26] The analytic BOP was derived from two-center, orthogonal tight binding theory and is described in detail elsewhere.[27] An optional electron counting (EC) energy term that enables the BOP to reproduce HT (001) surface reconstructions[28,29] has also been developed and parametrized.[26,30] However, simulations presented here concentrate upon the LT growth region where the formation of complex HT surface reconstructions are hindered by the reduced atom mobility.[9] This, combined with the increased computational demands of the modified form of the potential, led us to conduct the studies reported here without the EC term. The potential energy and forces between atoms were analytically implemented in a Lagrangian MD code[31,32] in which the equations of particle motion were numerically solved at femtosecond time steps using a Nordsieck predictor corrector algorithm.[33]

The MD simulations were used to investigate the vapor deposition of homoepitaxial thin films on a (001) GaAs surface as well as single species impact dynamics. The thin film growth was performed on a 32 Å $\times$ 32 Å (64 atoms/layer) substrate, while single species impact studies utilized a smaller 16 Å $\times$ 16 Å (16 atoms/layer) substrate. During vapor deposition simulations, the initial surface had a $\beta(2\times4)$ arsenic-rich reconstruction with a 75% coverage of arsenic arranged in sets of three dimers.[28] The initial surface for the single impact calculations was either an arsenic-terminated (2×1) or a gallium-terminated (1×2) surface, which consisted of dimerized rows of either arsenic or gallium, respectively.

Significant heat is released when either arsenic (2.36 eV/atom at 298 K) or gallium (3.20 eV/atom at 298 K) vapor condenses on a GaAs (001) surface.[34] In order to dissipate this additional thermal energy during the growth of a thin film, the substrate was divided into three computational regions. The positions of the gallium and arsenic atoms in the bottom two layers were fixed to avoid substrate translation. The atoms in the four layers above this fixed region were thermally controlled using a Nosé-Hoover thermostat algorithm[35] set to the desired simulation temperature, and the atoms in the remaining top three layers were left thermally unconstrained. The thickness of the thermostatically regulated region was then allowed to grow proportionally to the number of atoms incorporated into the thin film so that the thickness of the unconstrained region remained approximately constant under epitaxial growth conditions.

Gallium atoms and arsenic dimers were introduced normal to the surface at random positions and with random dimer orientations. The initial translational kinetic energy of both species was set to 0.17 eV/atom. Arsenic dimers were given an internal vibrational energy but no initial angular momentum. This vibrational energy was introduced by stretching the dimer 4.9–5.4 % from its equilibrium bond length (2.12 Å).

During vapor deposition simulations, a gallium atom or an arsenic dimer was added every 1.4 ps/nm^2. Typically the equivalent of 14–22 Å (or 10–16 layers) of material was deposited during 10 ns of simulation. In experiments, atoms or molecules arrive about every millisecond per square nanometer.[3] Therefore, the time available for surface diffusion of an atom or molecule after the initial impact with the surface was significantly underestimated by these MD simulations.

The atom positions were tracked during the analysis of single impacts for 10^2–10^4 ps. Each collision was repeated 100–1000 times with different initial conditions (i.e., position on the surface and dimer orientation) for the vapor species. These calculations were repeated at 25 K intervals between 100 and 2400 K for different combinations of flux species and surface types (arsenic or gallium rich).

III. VAPOR DEPOSITION SIMULATIONS

A series of homoepitaxial growth simulations were performed using substrate temperatures T between 500 and 1500 K and As:Ga flux ratios R between 0.9 and 3.4. Examples of crystalline structures grown at (a) $T=850$ K and $R=1.17$ and (b) $T=1500$ K and $R=3.14$ are shown in Fig. 1. The number of atoms of each type (N_{Ga} and N_{As}) deposited during the thin film growth are determined by the flux ratio R and the number of deposition events n_d:

$$N_{\mathrm{Ga}} = \frac{2n_d}{2+R}, \tag{1}$$

$$N_{\mathrm{As}} = \frac{2n_dR}{2+R}. \tag{2}$$

For the simulations reported here, $n_d \approx 714$. Of the arsenic and gallium atoms deposited at 850 K, nearly 14% of the

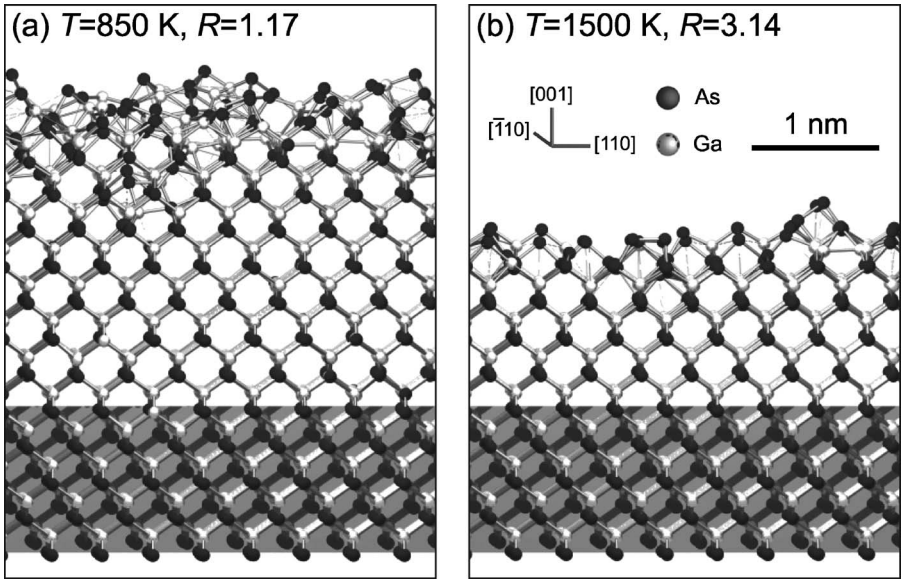

FIG. 1. As-grown GaAs thin film structures after 10 ns of deposition at (a) 850 and (b) 1500 K. The initial substrate is marked by the reflective plane. The atom positions, in the absence of vibrational displacement from the local low-energy sites, are shown.

arsenic atoms but none of the gallium atoms were desorbed. At 1500 K, more than 64% of the arsenic atoms and 1% of the gallium atoms desorbed. Because of this temperature-dependent arsenic desorption (discussed in greater detail later), the films grown at 850 and 1500 K have different thicknesses. Nevertheless, both as-grown films were stoichiometric, with roughly equal numbers of gallium and arsenic atoms, and they were both terminated by arsenic-rich surfaces.

The arsenic composition of many similarly deposited thin film samples was measured for 121 different combinations of the temperature T and As:Ga flux ratio R (see Fig. 2). Each of the films grown in these simulations was relatively thin; hence, any extra arsenic or gallium atoms on the surface affected the measured arsenic atomic composition values. Therefore, the arsenic atomic composition values had some variation between 0.50 and 0.53 for as-grown stoichiometric films. Within this range of film compositions, crystalline

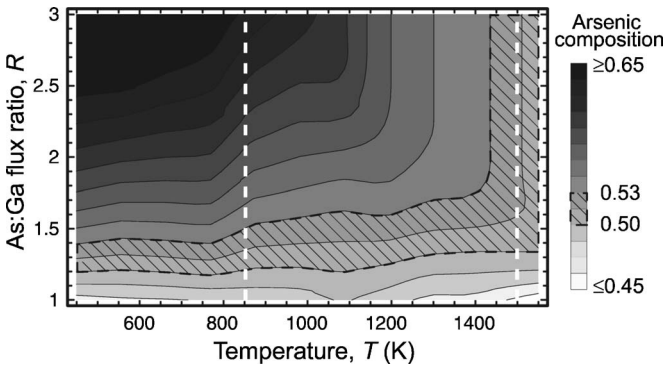

FIG. 2. Arsenic composition of as-grown thin films as a function of As:Ga flux ratio R and substrate temperature T. Arsenic-rich compositions are the darkest. The stoichiometric composition region ($0.50 \leqslant R \leqslant 0.53$) is shown with diagonal-hash lines. The composition along the white dashed lines are examined more fully in Fig. 3. Composition contours for $T \geqslant 1000$ K indicate a temperature-dependent critical flux ratio (kneelike bend), above which the film composition does not change.

films were always grown provided substrate temperatures were above 800 K.

Figure 2 exhibits several features that were consistent with experimental observations. Deposition at high temperatures (e.g., 1400–1500 K) resulted in stoichiometric films for all R values above 1.3, whereas LT deposition resulted in film compositions that were highly dependent upon the As:Ga flux ratio.[9] The simulations also revealed the existence of a critical value of R at each temperature above which the film composition depended weakly upon the composition of the vapor. This indicates the existence of an arsenic solubility limit above which the excess arsenic desorbs. We observed that more arsenic was soluble in the GaAs lattice as the substrate temperature decreased. A qualitatively similar limit has been observed experimentally.[12,36]

It is also evident in Fig. 2 that for a fixed flux ratio, the gallium concentration increased with growth temperature. Gallium-rich films were formed at all temperatures if $R \lesssim 1.2$. Both observations are also consistent with experiments, which indicate that gallium-rich surface structures are formed during HT deposition with low arsenic overpressures.[29] These results imply that the As_2 sticking ratio drops as the growth temperature is increased, which is also observed experimentally.[13]

The arsenic composition of thin films grown at 850 and 1500 K is plotted against the As:Ga flux ratio in Fig. 3. The arsenic atomic fraction is seen to increase with an increased As:Ga vapor flux ratio for deposition at 850 K. At high temperatures (e.g., 1500 K), the arsenic atomic fraction again initially increased with R but then reached a saturation value just above 0.50 at $R=1.3$. The dashed line in Fig. 3 corresponds to the anticipated arsenic atomic fraction if all atoms that arrived at the surface were incorporated into the thin film.

By examining the species involved in deposition and desorption during the growth process, it was observed that almost all gallium atoms were incorporated in the grown films for all temperatures and flux ratios explored in Fig. 3. The fraction of arsenic dimers incorporated into the film during growth appears to be dependent upon the concentration of

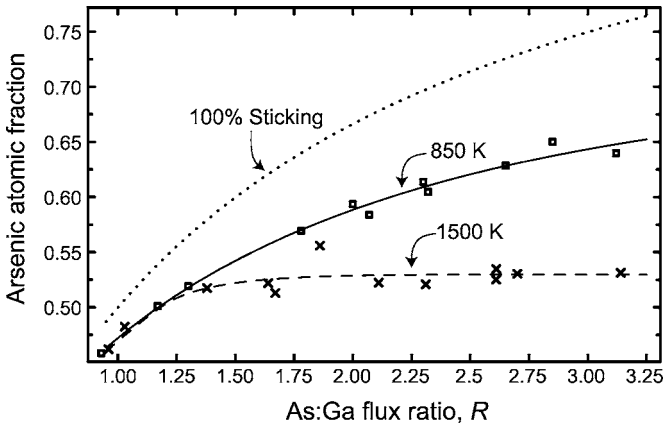

FIG. 3. The arsenic atomic fraction of thin films deposited at 850 and 1500 K. The dashed line indicates the theoretical arsenic concentration limit when the sticking fraction of both arsenic and gallium species is at unity.

arsenic in the As:Ga flux and the substrate temperature. Furthermore, as the growth temperature was decreased into the LT region, the fraction of As_2 vapor that bonded to the surface increased. However, even at the lowest simulation temperatures, approximately 15% of the arsenic dimers that initially impacted the surface were subsequently desorbed. Samples grown with low As:Ga flux ratios are therefore gallium rich. Examination of gallium-rich samples grown at $T \geqslant 800$ K, whose arsenic fractions lay between 0.45 and 0.50, indicate that the excess gallium was located on the free surface. The composition of the underlying film was stoichiometric in these cases; however, at lower temperatures, the stoichiometry changed and defects began to appear.

The composition trends of the simulated thin films were consistent with the experimental observations for both HT and LT growth regions. At low temperatures and arsenic-rich flux conditions, excess arsenic was incorporated into the deposited structures up to a temperature-dependent solubility limit, as observed experimentally.[9,12,36] At high temperatures and As:Ga flux ratios approaching unity, gallium-rich surfaces were observed to form in both simulations and experiments.[29] As the flux ratio was increased under HT growth conditions, the arsenic in excess of the stoichiometric value was desorbed resulting in stoichiometric films. This is also generally consistent with HT MBE results.[3] The simulated LT (800–1100 K) and HT (1400–1500+ K) conditions are thus phenomenologically linked to experimental LT (500–600 K) and HT (800–900 K) conditions. The higher simulated temperatures were a consequence of the accelerated deposition rate, which reduced the time available for surface diffusion during simulations. The longer diffusion distances occurring in experiments were approximately recovered in the simulations only by increasing the atomic mobility with an artificially higher substrate temperature.

IV. ARSENIC DIMER MECHANISMS

The vapor phase growth of GaAs involves the random impact of gallium atoms and arsenic dimers with a GaAs surface followed by adsorption, surface migration, and evaporation or molecular reactions on the surface leading to incorporation of gallium and arsenic in the lattice.[37] The mechanisms and rates of these kinetic processes are critical to a fundamental understanding of the epitaxial growth of GaAs films.[7] A kinetic model has been proposed for As_2 binding on the surface.[4,7,13,38–40] The model was motivated by As_2 sticking ratio observations on gallium-terminated (001), (110), and (111)A GaAs surfaces.[13,39,40] Various kMC simulations were also used to identify the states that best matched experimentally measured desorption rates, island nucleation kinetics, and terrace step growth rates.[15,16,38]

The kinetic model proposed the existence of (a) a weakly bound precursor state ($As_{2(p)}$) located relatively high above the surface, (b) a more strongly bound intermediate chemisorbed state ($As^*_{2(c)}$) located closer to the surface, and (c) an incorporated state ($As_{(i)}$) that has a bulk-lattice-like bond strength and interatom separations. The overall reaction can then be written as

$$As_{2(v)} \rightleftharpoons As_{2(p)} \rightleftharpoons As^*_{2(c)} \rightarrow 2As_{(i)}. \quad (3)$$

In the model, the incident vapor molecule ($As_{2(v)}$) is initially incorporated into the weakly bound precursor state ($As_{2(p)}$) from which it either desorbs to the vapor ($As_{2(v)}$) or becomes more strongly bound with the surface in an intermediate chemisorbed state ($As^*_{2(c)}$). An arsenic dimer in the $As^*_{2(c)}$ state then either returns to the $As_{2(p)}$ state or can be fully incorporated into the lattice ($As_{(i)}$).[40] These states represent classes of binding with a similar bond strength and distance from the surface. However, the structural configurations of the binding states are likely to depend upon the detailed atomic structure and composition of the surface.

The interplay between the states is directly affected by the temperature, the deposition rate, flux composition, surface composition, and surface structure.[4,40,41] Little is known about these effects on the specific binding states since the intermediate states cannot be observed directly in experiments due to the short state lifetimes.[42] Furthermore, kMC simulations are also unable to resolve these details due to the lack of lattice vibration in the model. However, the MD simulation approach detailed here can be used to directly study these intermediate states since its time resolution is $\sim 10^{-14}$ s and the BOP interatomic potential has been shown to capture the major bonding trends of the GaAs system.[26]

A. Gallium-terminated surfaces

The structure and reaction dynamics of the $As_{2(p)}$ and $As^*_{2(c)}$ states were explored for 10^4 ps following a dimer impact with the atoms of a perfect gallium-terminated (1×2) surface. This was accomplished by computing the dynamic dimer-surface binding energy and distance above the surface as a function of time following impacts with surfaces at temperatures between 300 and 1200 K. The dynamic dimer-surface binding energy ΔE was determined as the difference between the total energy of a system with a dimer in its bound position minus that of the same system with the fro-

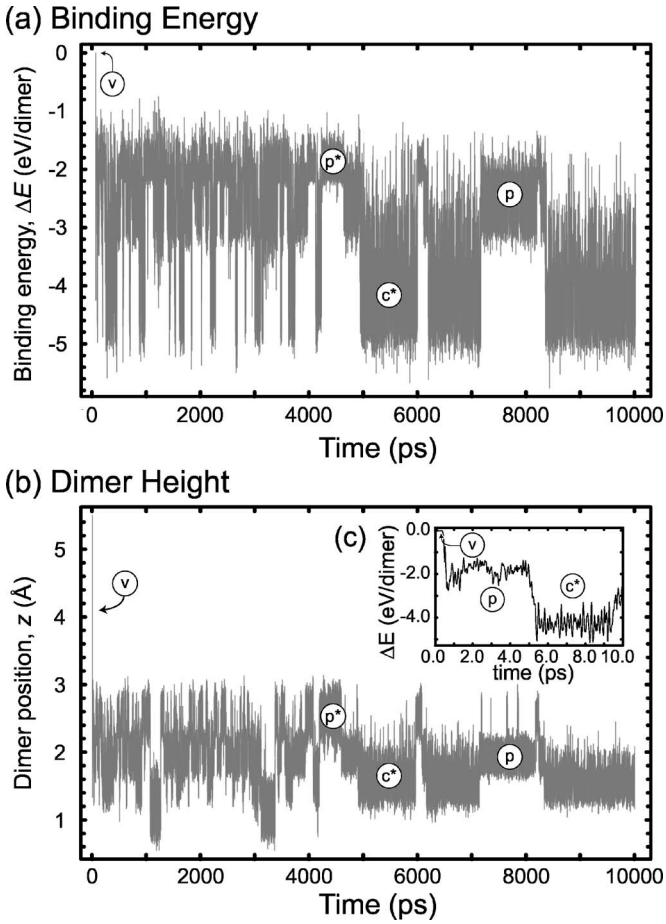

FIG. 4. Binding dynamics of As_2 on a gallium-terminated (1×2) surface at 900 K. (a) Dynamic binding energy (ΔE) of the arsenic dimer to the surface. (b) Vertical distance between the dimer center-of-mass and the (001) surface (z). The inset (c) shows the dynamic binding energy during the first 10 ps of interaction. Four states were observed and are marked by v, p^*, p, and c^*. The v state corresponds to a dimer in the vapor. The other states are transition states described in the text.

zen dimer removed beyond its interaction range with the surface (3.7 Å). The dynamic dimer-surface binding energy, or simply dynamic binding energy, is recorded every time step and is used to compute energy distributions over time. A dimer distance z above the surface was determined by calculating the difference between the location of the center-of-mass of the dimer and the position of the top layer of atoms forming the surface ($\approx$11.3 Å). As with ΔE, z was recorded at each time step and was used to monitor dimer-surface bonding behavior.

A typical result for an arsenic dimer impact with a gallium-terminated (1×2) surface at 900 K is shown in Fig. 4. The free vapor molecule (v) and three binding states (p, p^*, and c^*) can be identified in Fig. 4 based upon the arsenic dimer bond length, position above the substrate, and the dynamic binding energy with the surface. The v state corresponded to the free arsenic vapor where no interaction with the surface occurred [the $As_{2(v)}$ state in Eq. (3)]. In this case, $\Delta E=0$ eV/dimer and $z>3.7$ Å. In the vapor, the arsenic dimer had an interatomic spacing that vibrated around a mean length of 2.12 Å and a bond strength of 3.98 eV/dimer,[26] which are both consistent with experimental observations.[43] The three remaining states were involved in the dynamic binding of the arsenic dimer to the surface. Frequent switching between the p, p^*, and c^* binding states during the first 10^4 ps of interaction can be seen in Fig. 4.

The p^* state at 900 K corresponded to a dimer located at $z=2.28\pm0.44$ Å above the surface with a dynamic binding energy $\Delta E=-1.93\pm0.19$ eV/dimer. The bound As_2 molecule had an As-As separation distance of 2.21 ± 0.10 Å, less than 0.1 Å longer than that of the free As_2 molecule. Analysis of time resolved atom positions during the simulation showed that the dimer in the p^* state was strongly influenced by lattice vibration. A dimer on the (001) surface plane in the p^* state frequently switched between alignment with the [110] direction ($\pm18.6°$) (i.e., perpendicular to the surface dimer rows) and the $[\bar{1}10]$ direction ($\pm8.5°$) (i.e., parallel to the surface dimer rows). It resided in the [110] orientation 79% of the time and 21% of the time in the other $[\bar{1}10]$ orientation. The dimer axis in the p^* binding state remained within $\pm8.5°$ of the surface plane. Clearly, many different atomic configurations were associated with a similar dynamic binding energy and location above the surface. Nevertheless, the highly degenerate p^* state formed only two strong bonds with the surface. The structure was not stable and transferred to the p state (described below) when the system was relaxed at 0 K (to find the minimum-energy atomic positions).[44]

The arsenic dimer in the p state resided closer to the surface ($z=1.84\pm0.25$ Å) than in the p^* state and had a stronger dynamic binding energy ($\Delta E=-2.81\pm0.36$ eV/dimer). As with the p^* state, its dimer bond length (2.33 ± 0.12 Å) was similar to that of dimers in the vapor and it again formed only two strong bonds with the surface. Furthermore, the dimer axis remained in the (001) plane ($\pm7.3\%$) and resided in the [110] and $[\bar{1}10]$ orientations with equal probability. The distribution of orientations was much sharper than for the p^* state and only varied within $\pm7°$ in each direction at 900 K. Total energy minimization at 0 K of the p state configurations identified an example structure shown in Fig. 5(a). The long bond lengths and weak dynamic binding energy of the p state corresponded well with the $As_{2(p)}$ state in Eq. (3). The p^* state ($As^*_{2(p)}$) therefore appears to be a vibrationally excited version of the $As_{2(p)}$ state that exists when significant thermal energy is transferred into the dimer.

The c^* dynamic binding energy in Fig. 4 is -4.28 ± 0.31 eV/dimer, which was the lowest energy binding state observed. The dimer separation distance was 2.54 ± 0.11 Å and it was located at a height $z=1.54\pm0.15$ Å above the surface. This is relatively close to the interplanar spacing in the [001] direction of the bulk crystal (1.4 Å). This is consistent with c^* being a chemisorbed state and corresponds to the $As^*_{2(c)}$ state in Eq. (3). During simulations at 900 K, this state was oriented in the $[\bar{1}10]$ direction ($\pm5°$) nearly 100% of the time and remained almost parallel ($\pm5.3\%$) with the (001) surface. The typical structure of this state is shown in its relaxed form in Fig. 5(b). In this configuration, the arsenic dimer formed four strong covalent bonds with the surface. Before the arsenic dimer was added,

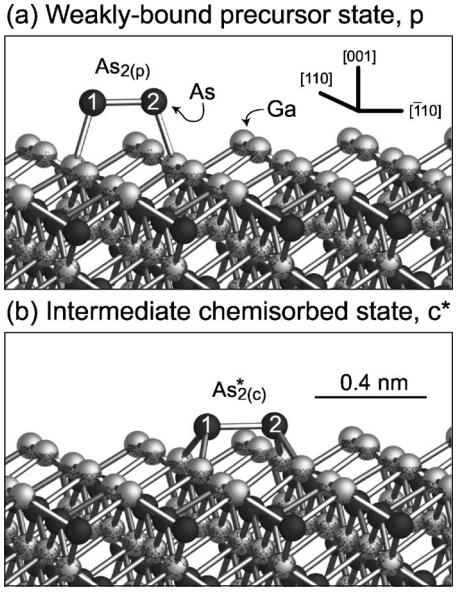

FIG. 5. Local atomic configurations for As_2 on a gallium-terminated (1×2) surface. (a) The weakly bound precursor state $(As_{2(p)})$ and (b) the intermediate chemisorbed state $(As^*_{2(c)})$. The configurations correspond to those obtained after total energy minimization at 0 K.

the surface gallium atoms were arranged in dimerized rows. However, in the $As^*_{2(c)}$ state, Fig. 5(b) shows that the surface Ga-Ga bonds directly below the arsenic molecule were broken and these two atoms moved into bulk latticelike positions.

At 1100 and 3300 ps in Fig. 4(b), the dimer position dropped to ~1 Å above the surface. Upon inspection of these states, it was found that the structure was very close to that of the $As^*_{2(c)}$ state. However, one of the surface dimers had been slightly displaced by thermal vibration, which allowed the dimer to move in the $[00\bar{1}]$ direction about 0.5 Å, since this anomaly was strictly a function of temporary changes in surface structure and does not define a new binding state.

The initial interactions between an arsenic dimer and a gallium-terminated surface at 900 K, Fig. 4(c), proceed according to the following sequence. At $t=0$, an incident dimer $(As_{2(v)})$ located beyond the interaction range ($z>5$ Å) of the potential has a dynamic binding energy of $\Delta E=0$. As the dimer approaches the surface, it becomes weakly bound to the surface in the $As_{2(p)}$ state. The $As_{2(p)}$ state was occupied for a short, random time (5 ps in Fig. 4) before transition to a more strongly bound state occurred. This more strongly chemisorbed state is the $As^*_{2(c)}$ state in Eq. (3). Analysis of multiple impacts indicated that the residence time in the $As_{2(p)}$ state depended upon the initial orientation of the dimer, the local surface structure at the impact site, and the surface temperature.

After the initial impact at 900 K, the dimer was observed to be highly mobile during the transition between binding states and it readily diffused across a gallium-terminated surface. During the migration of the dimer on the surface, the

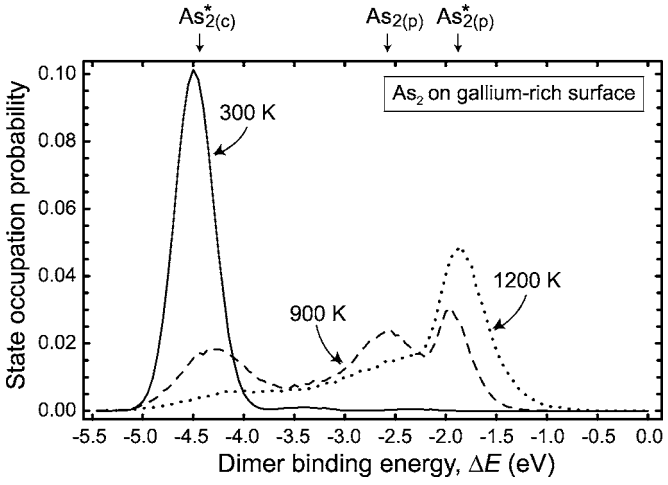

FIG. 6. The dynamic binding state occupation probability distribution at 300, 900, and 1200 K during 10^4 ps of dimer/surface binding.

fraction of time occupied by each state was determined by calculating the area under the state occupation probability curve. The division line between the $As^*_{2(c)}$ and $As_{2(p)}$ states was selected at −3.65 eV/dimer, while −2.26 eV/dimer was used to divide the $As_{2(p)}$ and $As^*_{2(p)}$ states. These state occupation probabilities are shown at 300, 900, and 1200 K in Fig. 6.

At 300 K, the incorporated dimer resided in the $As^*_{2(c)}$ state for the majority of the time (98.4%) and only briefly occupied either the $As_{2(p)}$ (1.4%) or $As^*_{2(p)}$ (0.2%) states. Hence, the intermediate chemisorbed state $(As^*_{2(c)})$ was the dominant state at low temperatures. As the temperature was increased to 900 K, the switching between the $As^*_{2(p)}$, $As_{2(p)}$, and $As^*_{2(c)}$ states increased in frequency (3 transitions/ns in Fig. 4). The strongly bound $As^*_{2(c)}$ state was occupied for 32.1% of the time, while the weakly bound states were occupied 40.5% $(As_{2(p)})$ and 27.4% $(As^*_{2(p)})$ of the time. Clearly, the occupation probability favored the two weakly bound states $(As^*_{2(p)}$ and $As_{2(p)})$ as temperatures neared the upper limit of experimental MBE growth.[3] At 1200 K, the weakly bound $As^*_{2(p)}$ state had the highest occupation probability (58.3%), followed by the $As_{2(p)}$ (30.2%) and the $As^*_{2(c)}$ (11.5%) states. The dimer had a very high switching frequency (>30 switchings/ns) between each of these states. At such high temperatures, the four strong bonds of the $As^*_{2(c)}$ state could not be sustained and lattice vibrations led to desorption from the $As^*_{2(p)}$ state.

The MD analysis of atomic assembly processes is generally consistent with the kinetic model of Eq. (3). A variant of the $As_{2(p)}$ state $(As^*_{2(p)})$ was observed to have a high occupancy probability at high temperatures. At lower temperatures, the $As^*_{2(c)}$ state had high occupancy. It was clear from the MD simulations that the transition between the $As^*_{2(c)}$, $As_{2(p)}$, and $As^*_{2(p)}$ states was completely reversible and occurred repeatedly as the dimer diffused across the surface.

B. Arsenic-terminated surfaces

Experimental observations of the interaction of arsenic dimers with arsenic-terminated surfaces indicate that the bonding is temporary unless temperatures are low and the arsenic concentration in the vapor is very high.[28,45] Unless these conditions exist, As_2 incorporation into the crystalline GaAs lattice requires surface accessible gallium adsorption sites.[4,7] However, under LT and high arsenic flux conditions, freely accessible gallium sites are rarely encountered and colder surfaces allow the binding of arsenic dimers to the arsenic-terminated surfaces. Under these conditions, the kinetic model developed for arsenic dimer binding to gallium-terminated surfaces [Eq. (3)] no longer applies.

Interactions between arsenic dimers and a perfect arsenic-terminated (2×1) surface were explored to investigate the binding states present during LT GaAs growth under high As:Ga flux ratio conditions. In contrast to the gallium-terminated surface, where impacting dimers were almost always bound to transition states, dimer adsorption/desorption was highly dependent upon the detailed structure at the impact site for arsenic-terminated surfaces, and the dimers orientation in the vapor state strongly influenced the adsorption probability.

Rapid desorption or occasional adsorption of arsenic dimers was observed when arsenic dimers impacted an arsenic-terminated surface. The dynamic binding energy and atom configurations for a typical rapid desorption event are shown in Fig. 7. The dimer in this simulation impacted the surface between the dimer rows and was initially nearly vertically oriented ($\approx30°$) to the surface, see part (1) of Fig. 7(b). Initially, atom 2 of the dimer impacted the surface between the dimer rows, where it briefly (and weakly) bonded with gallium atoms in the second layer below the surface and surface arsenic atoms [see part (2) of Fig. 7(b)]. The bonding was weak, Fig. 7(a), and the dimer quickly desorbed [see part (3) of Fig. 7(b)]. Throughout this event, atom 1 of the dimer remained well above the surface and bonded only with one surface arsenic atom [see parts (1)–(3) of Fig. 7(b)]. While this particular impact resulted in rapid desorption, similar impacts between the dimer rows sometimes resulted in kinetically trapped dimers whose desorption rate was then strongly dependent upon temperature. However, none of these interactions were observed to transition to or from the precursor state.

At 500 K, rapid desorption occurred in 18% of the more than 1000 surface impacts monitored. This rapid desorption from the arsenic-terminated surface is consistent with the observation that ~15% of the arsenic dimers did not stick to the surface during thin film growth simulations.

Surface adsorption of the arsenic dimers was observed to occasionally occur. An example at 500 K is shown in Fig. 8. Following impact, the dimer assumed a weakly bound configuration with a dynamic binding energy $\Delta E\approx-1.25$ eV/dimer, Fig. 8(a). The local atomic configuration of this state is shown in Fig. 8(b). The interatom separation within the dimer was 2.35 Å, compared to a separation of 2.12 Å in the vapor. The dimer in this precursor configuration was located ~2.1 Å above the surface. It did not perturb the original atomic surface structure and formed two

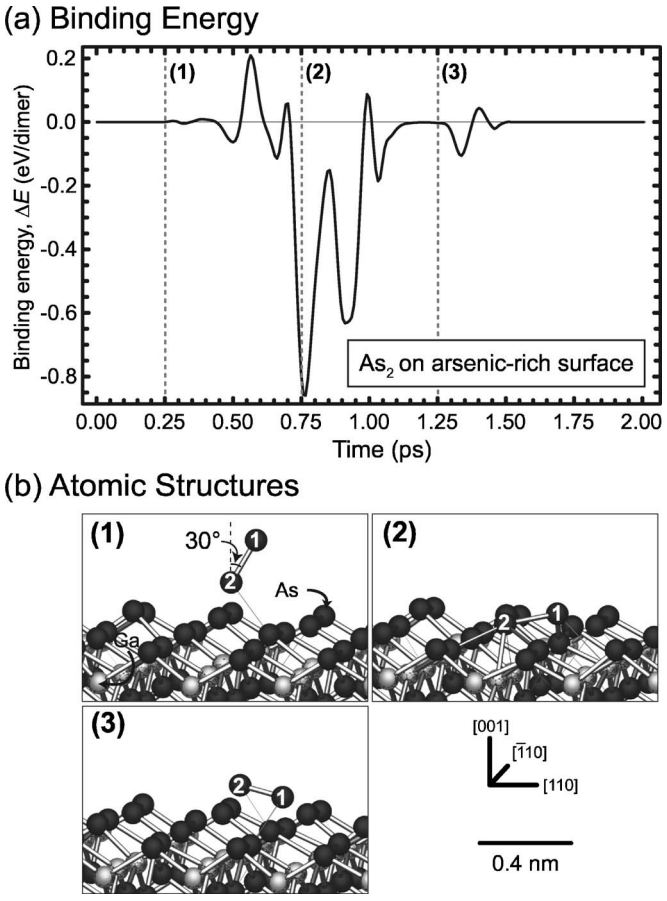

FIG. 7. A rapid As_2 desorption event from an arsenic-terminated (2×1) surface at 500 K. (a) The dynamic binding energy of the arsenic dimer to the surface for interaction after initial impact. (b) The local atomic configurations at (1) 0.25 ps, (2) 0.75 ps, and (3) 1.25 ps are also shown. The initial dimer angle is measured with respect to the axis perpendicular to the (001) surface.

strong bonds with the arsenic-rich surface. However, the dimer spacing is ~0.2 Å longer and ~0.4 Å closer to the surface than the *ab initio* values reported at 0 K.[17] Nevertheless, the short dimer spacing and weak bonding are characteristics that are roughly analogous to the weakly bound precursor state ($As_{2(p)}$) in Eq. (3).

The second state indicated in Fig. 8(a) had much stronger dynamic binding energy ($\Delta E=-3.09$ eV/dimer at 500 K) and resided closer to the surface ($z=1.84$ Å) compared to the $As_{2(p)}$-like state. The atomic configuration for this second state is shown in Fig. 8(c). Four relatively strong bonds were formed with the surface. The As-As-As bond angles between the dimer and the surface were approximately 90°. The As-As dimer interatomic spacing was 2.45 Å when bonded to the arsenic-terminated surface. This state is somewhat similar to the intermediate chemisorbed state ($As^*_{2(c)}$) seen in the gallium-terminated surface since it has a high average dynamic binding energy and short bond lengths. However, the dimer did not open up the substrate dimers, as observed during adsorption on gallium-terminated surfaces. Hence, this $As^*_{2(c)}$-like adsorbed state is identified as $As^*_{2(a)}$ within this paper.

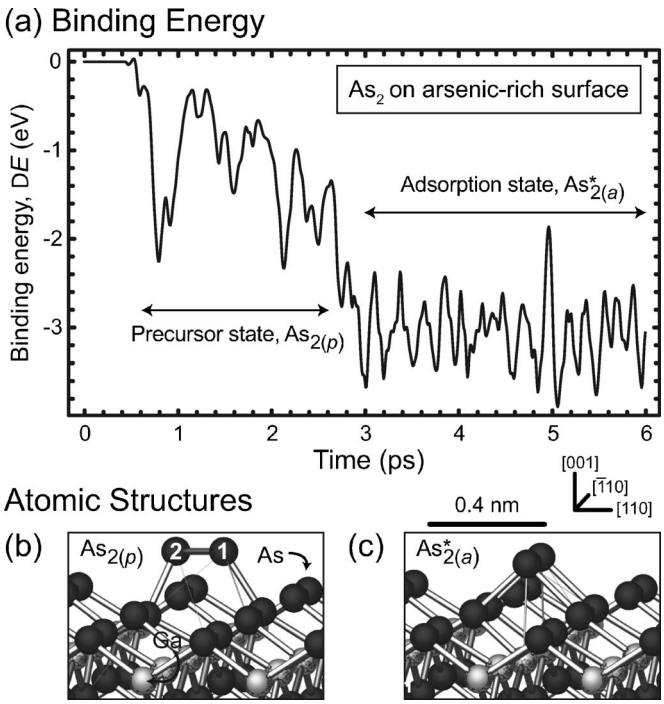

FIG. 8. Adsorption of As_2 onto the arsenic-terminated (2×1) surface at 500 K. (a) The dynamic binding energy of the arsenic dimer for 6 ps of interaction after impact. Atomic structures of (b) the weakly bound precursor and (c) the adsorbed states are also shown.

The dynamic binding energy (ΔE), lateral in-plane position of the arsenic dimer on the surface, and the dimer distance above the surface (z) were studied for the $As^*_{2(a)}$ state between 300 and 1200 K for times up to 10^4 ps. Unlike the gallium-terminated case, no switching between states was observed beyond the initial $As_{2(p)}$ to $As^*_{2(a)}$ transition. Once in the $As^*_{2(a)}$ state, the dimer atoms vibrated with a temperature-dependent amplitude, and little surface migration of the dimers was observed within the 10^4 ps calculation window. Instead of diffusing, the dimers tended to desorb when thermally perturbed from the $As^*_{2(a)}$ state.

C. Dynamic As-As bond length trends

To understand the variation of the As-As dimer bond length for different surface-bonding configurations, the correlation between As-As dimer bond length and the distance of the dimer above the surface is shown in Fig. 9 for selected bonding states on gallium- and arsenic-terminated surfaces at temperatures of 300, 600, 900, and 1200 K. Some unstable bonding states are not selected because they occur at a low frequency. For instance, the $As_{2(p)}$ and $As^*_{2(p)}$ states at 300 K and the $As^*_{2(c)}$ state at 1200 K, respectively, are omitted for the gallium-terminated surface. Likewise, only the $As^*_{2(a)}$ state is displayed for the arsenic-terminated surface, as it is the only state regularly occupied during dynamic dimer bonding below 1200 K.

It can be seen from Fig. 9 that although there is a small oscillation, all the dimer bond lengths and the distances of

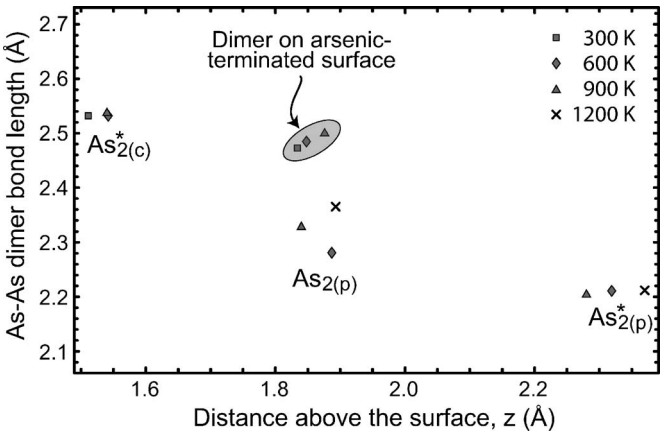

FIG. 9. Mean As_2 dimer bond length as function of system temperature and bonding state. Dimer bonding data are shown for the gallium-terminated surface, except when noted for the arsenic-terminated surface in the shaded oval. Some 300 and 1200 K states are not shown due to limited occupancy times and, thus, little or no data are available under these conditions.

the dimer above the surface appear to be unique to the surface type, bonding state, and temperature. On the gallium-terminated surface, the As-As dimer bond length successively decreases for the bonding states ($As^*_{2(c)}$, $As_{2(p)}$, and $As^*_{2(p)}$).

In general, the bond length between a pair of atoms is indicative of the bond strength: the shorter the bond length, the stronger the bond. Because the bond order describes the number of electrons in the antibonding state minus the number of electrons in the bonding state, its value increases when the bonding strength increases. The bond order of a free As_2 molecule is greater than one because electrons freely participate in the σ and π bonding. This large bond order gives rise to a strong bonding and a short interatomic separation distance within the dimer. The bond strength weakens and bond length increases when the As-As dimer approaches a surface because electrons are distracted by the formation of additional bonds with the surface. The bond orders of the As-As dimer bond and the newly formed bonds, however, depend not only on the number of the new bonds, but also the associated bond angles. As a result, the average As-As bond length is dependent on the surface type and bonding state. This effect is well captured by our bond order potential, which is not only formulated based on the fundamental first principles,[46] but also parametrized to well predict the cohesive energies of various bulk crystals that sample a variety of coordinations and bond angles.[26]

V. STICKING RATIO ESTIMATES

A. Gallium- and arsenic-terminated surfaces

Arsenic and gallium desorption rates from (001) GaAs surfaces depend on the surface structure, adsorbate coverage and species type, and the surface temperature. These rates are influenced by the binding states that the incoming species occupy, see Eq. (3).[13] During growth, the impacting species

that bind to the surface migrate on the surface until they encounter a surface site that traps the atom or dimer. On a flat gallium-terminated surface, the migration of an arsenic dimer was observed to be quite significant. In this case, the effective migration time between impact and incorporation into the film (usually at a terrace ledge) has a significant impact on growth kinetics.[38] On the other hand, our observations of arsenic dimer-surface binding on a flat arsenic-terminated surface showed rapid desorption and little surface migration once the arsenic dimer occupied the $As^{*}_{2(a)}$ state. Nevertheless, the surface residence time (even for a relatively small number of surface binding sites) can still have a significant impact on the growth dynamics of GaAs thin films. We can explore the connection between surface migration (residence) time and desorption using perfectly flat gallium-terminated (1×2) and arsenic-terminated (2×1) surfaces. These surfaces represent simple approximations to the gallium- and arsenic-rich surfaces observed experimentally for (001) surface reconstructions.[28,29,42]

The arsenic dimer and gallium atom adsorption and desorption behaviors have been measured by monitoring the behavior of several thousand impacts on gallium- and arsenic-terminated surfaces as a function of temperature and counting the fraction of arsenic dimers and gallium atoms that desorb. These data were converted into a sticking ratio S_R which can be computed by dividing the number of atoms that remained on the surface by the number that impacted the surface in a prescribed time. The gallium atom sticking ratio on both gallium- and arsenic-terminated surfaces was found to be close to unity between 100 and 2000 K. No significant gallium desorption was observed within 100 ps of the impact event on either surface; however, significant arsenic desorption was observed from the upper substrate layers as the temperature was increased above 1650 K. Hence, the sticking ratio estimates here focus on the arsenic dimer, where variation as a function of temperature is clearly observed. These calculations can be compared to experimentally determined sticking ratio data for arsenic dimer impacts on gallium-terminated (4×2) surfaces.[13]

The arsenic sticking fraction on (1×2) and (2×1) surfaces is shown in Fig. 10. The sticking ratio data points (black dots) were obtained from an analysis of 100–200 dimer impacts at temperatures between 100 and 2400 K. Each impact event was monitored for desorption for 100 ps. The estimated sticking ratio had a standard deviation around ±10%.[47]

The evaluation of the sticking ratio as a function of time t and temperature T requires the utilization of a time dependent kinetic model. To this end, consider a flat (001) GaAs surface that has N_J dimer impacts per unit area from an incoming flux. From these incoming dimers, N_0 dimers per unit area bind to the surface and are assumed not to interact with each other. The ratio N_0/N_J is a short time ($t\sim0.1$ ps or less) sticking coefficient, which is approximated by the data obtained from MD.

A kinetic model can be used to determine the number of dimers per unit area that remain on the surface as a function of time. The purpose of this model is to extrapolate the short-time sticking coefficient calculated in the simulation to a more realistic time scale sticking coefficient.

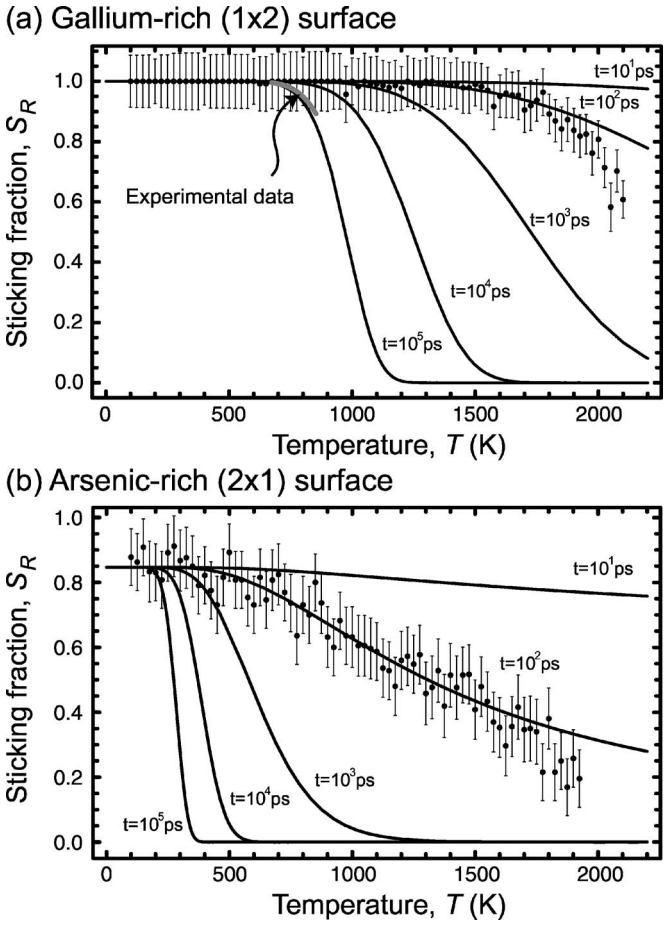

FIG. 10. The temperature dependence of the sticking ratio of an As_2 vapor flux on (a) a gallium-terminated (1×2) surface and (b) an arsenic-terminated (2×1) surface. Experimental sticking ratio data for As_2 on a gallium-rich (4×2) surface (Ref. 13) is shown as a thick gray line in part (a). The time-dependent desorption trends are plotted for a wide range of surface migration times with solid black lines.

Experimental studies suggest As_2 desorption exhibits first order reaction kinetics.[13,42] The desorption rate of an adsorbate dimer R_d can therefore be written

$$R_d = -dN/dt = kN, \tag{4}$$

where k is the rate constant for the desorption process and N is the number of dimers per unit area on the surface at time t. The rate constant k can be expressed in an Arrhenius form

$$k = A_x \exp(-Q_x/k_BT), \tag{5}$$

where Q_x is the activation barrier for arsenic dimer desorption from a surface of type x, A_x is the pre-exponential factor for a surface of type x, k_B is the Boltzmann constant, and T is the absolute temperature of the system.

The number of dimers that remain on the surface per unit area at time t can be found by integrating the desorption rate equation in Eq. (4):

$$N(t) = N_0 \exp(-kt). \quad (6)$$

The arsenic dimer sticking ratio S_R can then be calculated by

$$S_R = \frac{N(t)}{N_J} = \frac{N_0}{N_J} \exp(-kt), \quad (7)$$

where $N_0/N_J=1$ when all the dimers initially bind to the surface [as is the case for the (1×2) surface] and $N_0/N_J<1$ when a rapid desorption mechanism is in play [as is the case on the (2×1) surface, where $N_0/N_J\approx0.847$].

The desorption activation energies and pre-exponential factor can be fitted to the simulated As_2 sticking ratio data as a function of temperature on both the gallium-terminated (1×2) and arsenic-terminated (2×1) surfaces for $t=100$ ps. This gives $A_{1\times2}=0.269$ ps^{-1}, $Q_{1\times2}=0.886$ eV (on a gallium-terminated surface), $A_{2\times1}=0.0329$ ps^{-1}, and $Q_{2\times1}=0.206$ eV (on an arsenic-terminated surface). The $t=100$ ps curve begins to deviate from the simulated data at temperatures above 1700 K due to the evaporation of arsenic from the initial gallium- and arsenic-terminated substrates.

Experimental data for the arsenic sticking fraction on a (4×2) gallium-rich surface have been obtained between 673 and 853 K for deposition rates between 5×10^{14} atoms/cm^2 s and 9×10^{14} atoms/cm^2 s.[13] These data are well fitted by Arrhenius relations [solid gray line in Fig. 10(a)] for a kinetic model similar to that in Eq. (3). The arsenic sticking ratio predicted by our kinetic desorption model can be plotted for a range of surface residence (or free migration) times, see Fig. 10. The experimental sticking ratio data for As_2 on a gallium-rich surface is consistent with the predictions from our kinetic model if the time over which desorption can occur is increased from 10^2 to 10^5 ps. However, it should be noted that due to the simplicity of the (1×2) gallium-terminated surface used in this model, the 10^5 ps free migration time predicted is likely underestimated for surfaces with defect sites, as is the case for real (4×2) surfaces.[29]

The experimental model used to fit the experimental sticking ratio data to Arrhenius relations assumes binding states similar to those of Eq. (3).[13] The desorption activation barrier (Q_d) from these states was evaluated and fitted to the Arrhenius relation $Q_d\approx0.91\pm0.08$ eV.[13] The magnitude indicated that desorption most likely occurred from the strongly bound $As^*_{2(c)}$ state.[13] In our time-dependent model, the desorption activation barrier energy for arsenic was 0.886 eV and was consistent (by virtue of magnitude) with desorption from the $As^*_{2(c)}$ state, which matches well with the experimental estimate. This insight can be coupled with the direct observation of arsenic dimer interactions on the (1×2) gallium-terminated surface. In these dynamic simulations, the dimer frequently switched between the $As^*_{2(p)}$, $As_{2(p)}$, and $As^*_{2(c)}$ states. Furthermore, the final desorption event was observed to occur from the $As^*_{2(p)}$ state. Nevertheless, desorption was not observed to occur from the weakly bound state without first going through the more strongly bound $As^*_{2(c)}$ state. Therefore, a relatively high activation energy barrier for desorption is expected despite the common occurrence of the $As^*_{2(p)}$ and $As_{2(p)}$ states.

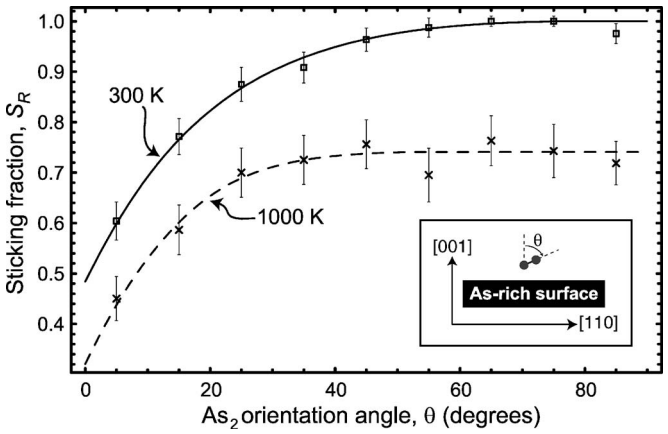

FIG. 11. Sticking ratio of As_2 on the arsenic-terminated (2×1) surface as a function of the initial orientation angle of the dimer to the axis perpendicular to the (001) surface. Measurements are reported at 300 and 1000 K.

The experimental study of As_2 interactions with an arsenic-rich surface shows that essentially no arsenic stays bound to a surface in the absence of exposed gallium atoms at high temperatures.[4,7] However, arsenic has been observed to stick at temperatures below 750 K in an arsenic-rich environment.[48] The low desorption energy barrier predicted in this model indicates that As_2 readily desorbs in accordance with experimental observations. This is consistent with easy desorption from a weakly bound precursor state.[17] Here, we have accounted for two paths to desorption that contribute to this barrier. These paths of rapid desorption and thermally activated desorption are consistent with our mechanistic observations in the previous section. Hence, the time resolved kinetic model identifies a correspondence between the simulations and experiments. This, in combination with the mechanistic insights about the binding of As_2 dimers to the (001) GaAs surface, provides insight into the states that are otherwise not observable experimentally.

B. Arsenic dimer orientation effects

Since diffusion of the dimer on arsenic-terminated (2×1) surfaces was significantly less than on a gallium-terminated surface, the local surface structure of the impact site and orientation more strongly influence the probability of binding in the $As^*_{2(a)}$ state. For the simple dimer-row surface structure, the issue reduces to whether a dimer impacts the top of the dimer row $(As_{2(p)}\rightarrow As^*_{2(a)})$ or within the narrow trench between the rows (rapid desorption or trapping). The orientation effect was quantified by analyzing the sticking ratio of As_2 on an arsenic-terminated surface at 300 and 1000 K, see Fig. 11.

The sticking ratio data were calculated by repeating 1000–1500 single impact runs with randomized orientation and location over a (2×1) surface with surface temperatures between 300 and 1500 K. After the introduction of the dimer, the system was allowed to progress for 100 ps, as before.

The sticking ratio was then calculated as a function of the initial dimer orientation angle and averaged in each of the 9 orientation angle bins between 0 and 90°. Figure 11 shows that dimers initially perpendicular to the surface ($\theta < 40°$) were 40% more likely to desorb than impacts where both dimer atoms reached the surface nearly simultaneously ($\theta > 40°$). The desorption rate was therefore a strong function of angle in a scenario without angular momentum. A similar study was performed for As_2 on the gallium-terminated (1 $\times$2) surface and no appreciable sticking preference based on initial angle was seen.

VI. CONCLUSIONS

(1) A GaAs bond-order potential (BOP) based molecular dynamics (MD) method has been demonstrated to reproduce phenomenological observations of the high- and low-temperature growth of GaAs on the (001) surface.

(2) The calculated arsenic composition of the as-grown thin films was strongly dependent on temperature and As:Ga flux ratio. The experimental temperature-dependent arsenic solubility trend was reproduced with the GaAs BOP-based MD method.

(3) The interaction of As_2 on a gallium-terminated (1 $\times$2) surface was observed to match a proposed kinetic model quite well. An additional excited precursor state was observed during the significant switching between the precursor and intermediate chemisorbed states. This switching was temperature dependent and was significant at growth temperatures commonly used in experiments.

(4) Arsenic dimers can adsorb to the arsenic-terminated surface and generally diffuse much less than those on a gallium-terminated surface. Rather than diffusing, dimers are found to simply desorb once perturbed from their binding state.

(5) A correspondence between simulated and experimental sticking ratio values was established by utilization of a time-dependent kinetic model for desorption. The arsenic dimer surface migration time was found to have a significant influence on the desorption rate.

(6) The sticking of As_2 on an arsenic-terminated surface is strongly dependent upon the orientation of the dimer at the time of impact. No such dependence was observed on the gallium-terminated surface.

ACKNOWLEDGMENTS

We acknowledge the Defense Advanced Research Projects Agency and Office of Naval Research (C. Schwartz and J. Christodoulou, Program Managers) for support of this work under Contract No. N00014-03-C-0288. We are grateful to M. M. Morgan and A. S. Grimshaw of the Virginia Center for Grid Research at the University of Virginia for their generous allotment of computing time (more than 11 years of processor time) on the 64-node Centurion Opteron cluster.

*Author to whom correspondence should be addressed. Electronic address: murdick@mailaps.org

[1] R. Kaspi, in *Properties of Gallium Arsenide*, edited by M. R. Brozel and G. E. Stillman, 3rd ed. (INSPEC, London, 1996), Vol. 16, pp. 601–607.
[2] A. Y. Cho, J. Vac. Sci. Technol. **16**, 275 (1979).
[3] R. Evans, in *Properties of Gallium Arsenide*, edited by M. R. Brozel and G. E. Stillman, 3rd ed. (INSPEC, London, 1996), Vol. 16, pp. 655–661.
[4] C. T. Foxon and B. A. Joyce, Surf. Sci. **64**, 293 (1977).
[5] J. M. Van Hove and P. I. Cohen, Appl. Phys. Lett. **47**, 726 (1985).
[6] J. R. Arthur, J. Appl. Phys. **39**, 4032 (1968).
[7] J. R. Arthur, Surf. Sci. **43**, 449 (1974).
[8] G. R. Bell, T. S. Jones, and B. A. Joyce, Surf. Sci. **429**, L492 (1999).
[9] M. Missous, in *Properties of Gallium Arsenide*, edited by M. R. Brozel and G. E. Stillman, 3rd ed (INSPEC, London, 1996), Vol. 16, pp. 679–683.
[10] M. Missous and S. O'Hagan, J. Appl. Phys. **75**, 3396 (1994).
[11] K. Mahalingam, N. Otsuka, M. R. Melloch, J. M. Woodall, and A. C. Warren, J. Vac. Sci. Technol. B **9**, 2328 (1991).
[12] M. Kaminska, E. R. Weber, Z. Liliental-Weber, R. Leon, and Z. U. Rek, J. Vac. Sci. Technol. B **7**, 710 (1989).
[13] E. S. Tok, J. H. Neave, J. Zhang, B. A. Joyce, and T. S. Jones, Surf. Sci. **374**, 397 (1997).
[14] V. Avrutin, D. Humienik, S. Frank, A. Koeder, W. Schoch, W. Limmer, R. Sauer, and A. Waag, J. Appl. Phys. **98**, 023909 (2005).
[15] M. Itoh, G. R. Bell, A. R. Avery, T. S. Jones, B. A. Joyce, and D. D. Vvedensky, Phys. Rev. Lett. **81**, 633 (1998).
[16] M. Itoh, Prog. Surf. Sci. **66**, 53 (2001).
[17] C. G. Morgan, P. Kratzer, and M. Scheffler, Phys. Rev. Lett. **82**, 4886 (1999).
[18] P. Kratzer, E. Penev, and M. Scheffler, Appl. Surf. Sci. **216**, 436 (2003).
[19] J. G. LePage, M. Alouani, D. L. Dorsey, J. W. Wilkins, and P. E. Blöchl, Phys. Rev. B **58**, 1499 (1998).
[20] R. Car and M. Parrinello, Phys. Rev. Lett. **55**, 2471 (1985).
[21] M. C. Payne, M. P. Teter, D. C. Allan, T. A. Arias, and J. D. Joannopoulos, Rev. Mod. Phys. **64**, 1045 (1992).
[22] F. Gygi and G. Galli, Mater. Today **8**, 26 (2005).
[23] M. A. Salmi, M. Alatalo, T. Ala-Nissila, and R. M. Nieminen, Surf. Sci. **425**, 31 (1999).
[24] D. A. Murdick, X. W. Zhou, and H. N. G. Wadley, J. Cryst. Growth **286**, 197 (2006).
[25] D. A. Murdick, X. W. Zhou, and H. N. G. Wadley, Phys. Rev. B **72**, 205340 (2005).
[26] D. A. Murdick, X. W. Zhou, H. N. G. Wadley, D. Nguyen-Manh, R. Drautz, and D. G. Pettifor, Phys. Rev. B **73**, 045206 (2006).
[27] R. Drautz, D. A. Murdick, D. Nguyen-Manh, X. Zhou, H. N. G. Wadley, and D. G. Pettifor, Phys. Rev. B **72**, 144105 (2005).
[28] Q.-K. Xue, T. Hashizume, and T. Sakurai, Appl. Surf. Sci. **141**, 244 (1999).
[29] M. Pristovsek, S. Tsukamoto, A. Ohtake, N. Koguchi, B. G. Orr,

W. G. Schmidt, and J. Bernholc, Phys. Status Solidi B **240**, 91 (2003).
[30] X. W. Zhou, D. A. Murdick, and H. N. G. Wadley, J. Appl. Phys. **99**, 064908 (2006).
[31] M. Parrinello and A. Rahman, J. Chem. Phys. **76**, 2662 (1982).
[32] J. R. Ray and A. Rahman, J. Chem. Phys. **80**, 4423 (1984).
[33] A. Nordsieck, Math. Comput. **16**, 22 (1962).
[34] O. Kubaschewski, C. B. Alcock, and P. J. Spencer, *Materials Thermochemistry*, 6th ed. (Pergamon Press, New York, 1993), pp. 1–27.
[35] W. G. Hoover, Phys. Rev. A **31**, 1695 (1985).
[36] A. Suda and N. Otsuka, Surf. Sci. **458**, 162 (2000).
[37] A. Madhukar, Surf. Sci. **132**, 344 (1983).
[38] A. Madhukar and S. V. Ghaisas, CRC Crit. Rev. Solid State Mater. Sci. **14**, 1 (1988).
[39] E. S. Tok, J. H. Neave, F. E. Allegretti, J. Zhang, T. S. Jones, and B. A. Joyce, Surf. Sci. **371**, 277 (1997).
[40] E. S. Tok, T. S. Jones, J. H. Neave, J. Zhang, and B. A. Joyce, Appl. Phys. Lett. **71**, 3278 (1997).
[41] J. H. Neave, P. J. Dobson, B. A. Joyce, and J. Zhang, Appl. Phys. Lett. **47**, 100 (1985).
[42] S. Y. Karpov and M. A. Maiorov, Surf. Sci. **344**, 11 (1995).
[43] K. P. Huber and G. Herzberg, *Molecular Spectra and Molecular Structure: IV. Constants of Diatomic Molecules* (Van Nostrand Reinhold Company, New York, 1979), Vol. 4.
[44] W. H. Press, *Numerical Recipes in Fortran 77: The Art of Scientific Computing*, 2nd ed. (Cambridge University Press, New York, 1996).
[45] D. K. Biegelsen, R. D. Bringans, J. E. Northrup, and L. E. Swartz, Phys. Rev. B **41**, 5701 (1990).
[46] D. G. Pettifor, *Bonding and Structure of Molecules and Solids* (Oxford University Press, Oxford, 1995).
[47] J. R. Taylor, *An Introduction to Error Analysis*, 2nd ed. (University Science Books, Sausalito, California, 1997), pp. 245–255.
[48] A. Ohtake, M. Ozeki, T. Yasuda, and T. Hanada, Phys. Rev. B **65**, 165315 (2002).